

EFFICIENT ROTOR AERODYNAMIC SHAPE DESIGN USING A MULTI-FIDELITY NEURAL NETWORK-BASED GLOBAL OPTIMIZATION METHOD

Shuo Li[1,2], Wenping Song[1,2,*], Zhongqi Shen[1,2]

[1]Institute of Aerodynamic and Multidisciplinary Design Optimization, School of Aeronautics, Northwestern Polytechnical University, Xi'an 710072, China
[2]National Key Laboratory of Aircraft Configuration Design, Xi'an 710072, China

Abstract

The helicopter rotor is a critical component that determines the flight performance of a helicopter; therefore, aerodynamic shape design optimization of the rotor is of great significance for improving helicopter aerodynamic characteristics. However, conventional global optimization methods often face a dilemma: rotor aerodynamic design optimization based on high-fidelity numerical simulations is usually limited in efficiency due to the enormous computational cost, while fast evaluation methods, although efficient, cannot guarantee analysis accuracy and may lead to unreliable optimization results. To address this dilemma, this paper introduces a multi-fidelity neural network model and proposes a multi-fidelity data-driven modeling approach that can simultaneously satisfy the requirements on both optimization quality and efficiency. Based on this modeling approach, an efficient global aerodynamic shape design optimization method for a rotor is developed. First, an adaptive multi-fidelity neural network is improved in terms of network architecture and loss function, taking 17 geometric parameters as inputs that describe the rotor blade chord distribution, twist distribution, blade tip shape, as well as tip dihedral and anhedral. With these inputs, it enables efficient and accurate predictions of helicopter rotor thrust, torque, and moment coefficient. Subsequently, using the developed multi-fidelity neural network based genetic algorithm (GA), an aerodynamic shape design optimization is performed for a helicopter rotor, subject to constraints on rotor thrust, moment coefficient, and solidity, and with the objective of maximizing the figure of merit. High-fidelity numerical simulation of the optimized result shows that the optimized design obtained by the proposed method increases the figure of merit from the baseline 69.53% to 72.57%. Compared with the existing efficient global surrogate-based design optimization method using the Kriging model developed by our research group, the optimization quality is comparable, with a difference in the optimal figure of merit of only −0.08%, while the optimization efficiency is improved by a factor of about 82.5. Even when the time required for constructing the neural network dataset is included, the efficiency is still improved by a factor of about 16. The results validate the effectiveness of the proposed rotor aerodynamic shape design optimization method based on the multi-fidelity neural network model, demonstrating that the method can significantly enhance optimization efficiency while maintaining optimization quality.

Keywords: helicopter rotor; multi-fidelity neural network; efficient global design optimization method

1. Introduction

The helicopter is an aircraft with unique flight capabilities, featuring vertical take-off and landing, hovering, and low-speed forward or backward flight, which are generally not available in most fixed-wing aircraft [1]. Owing to its flexible flight modes, the helicopter has been widely used in both civil and military fields. The helicopter rotor is the core component of a helicopter, serving as both the primary lift source and the key control device, and it directly determines the overall performance of the helicopter [2]. At present, unconventional rotor configurations with features such as forward/backward sweep and dihedral/anhedral have demonstrated significant advantages in improving rotor aerodynamic performance, and have become the mainstream of modern rotor design,

with gradual adoption in practical helicopter applications. To fully exploit the potential of such unconventional configurations, aerodynamic shape design optimization methods have been continuously developed.

Since the late 1980s, a large number of research achievements have emerged in the field of rotor aerodynamic design optimization. Early studies mostly combined low-to-medium-fidelity aerodynamic models with gradient-based algorithms: Adelman et al. [3] employed the method of feasible directions and called the blade element momentum theory (BEMT) for iterative analysis; Khan et al. [4] also used the method of feasible directions but introduced a quasi-steady simplified Peters dynamic wake model; during the same period, Quackenbush et al. [5] attempted to couple the free vortex wake method with a linear optimization algorithm for rotor design optimization. Entering the 21st century, higher-fidelity CFD methods began to be introduced into the optimization loop. Yang et al. [6] adopted the Euler equations for CFD solutions in their optimization; Qian et al. [7] integrated the RANS equations with an SQP optimizer for rotor airfoil optimization. By the 2010s, RANS methods had become the widely used aerodynamic analysis tool in rotor design optimization, and the research focus shifted towards improving the optimization method itself, including increasing the number of design variables in global optimization methods and improving the efficiency of the optimization algorithm. However, due to the huge computational cost of high‑fidelity evaluations when used in global optimization, improving the efficiency of global optimization became a primary concern. Bu et al. [8,9] adopted the HK model-based global optimization method to perform rotor aerodynamic/acoustic design optimization, significantly improving the optimization efficiency using RANS Solver, and further developed it in 2022 into an efficient aerodynamic-structural-acoustic design optimization study for helicopter rotors with MHK model-based global optimization method using CFD-CSD coupled analysis solver. Zhang et al. [10] presented a multi-fidelity optimization method that first performs a low‑fidelity global scan of the design space, then uses high−fidelity RANS simulations coupled with gradient−based optimization, improved the performance of Skybus's propellers. In summary, rotor aerodynamic design optimization has gradually evolved from combining low-order aerodynamic models with gradient algorithms, through high-fidelity CFD solutions, to surrogate-assisted global optimization, continuously improving performance evaluation accuracy while steadily enhancing optimization efficiency and reliability. Nevertheless, these methods still rely on CFD solutions to varying degrees during the optimization process, and the enormous computational time required for high-fidelity evaluations has become a bottleneck for further improving optimization efficiency.

In recent years, artificial intelligence technology has offered new ideas for breaking through this bottleneck. With the advancement of AI, its application in the field of computational fluid dynamics has become increasingly widespread. Neural networks, as efficient surrogate models, can rapidly predict fluid flow results, significantly reducing the computational time and resources required by high-fidelity evaluation in the design optimization process. However, training an accurate neural network model requires a large amount of data. High‑fidelity data are often scarce and expensive, whereas low‑fidelity data can be obtained relatively cheaply. Therefore, Meng et al. [11] proposed a multi-fidelity deep neural network to capture the correlation between high‑ and low‑fidelity data. while low-fidelity data can be obtained relatively cheaply. Nevertheless, studies have shown that multi-fidelity neural networks are sensitive to the choice of regularization coefficients and still struggle to accurately fit complex nonlinear relationships, which directly limits the optimization quality and efficiency when they serve as surrogate models for rotor aerodynamic performance. To address this issue, based on existing research, this paper investigates improvement methods for the multi-fidelity neural network model, aiming to enhance its accuracy and robustness. The improved model is then applied to the prediction of helicopter rotor aerodynamic performance, exploring the technical pathway for effective integration between rotor global design optimization methods and neural network aerodynamic modeling. Furthermore, a global aerodynamic shape design optimization for rotors based on this multi-fidelity neural network model is carried out, followed by a systematic analysis of the resulting performance and optimization efficiency.

The remainder of this paper is organized as follows. Section 1 presents the introduction, which reviews the development status and existing problems of rotor design optimization methods and

neural network modeling approaches, and elaborates the research purpose and significance. Section 2 describes the improvements made to the existing multi-fidelity neural network model and its validation. Section 3 investigates the modeling method for the rotor performance prediction model, including verification of the high-fidelity CFD method, dataset construction, and discussion of the model architecture and training results. Section 4 outlines the optimization framework, formulates the optimization problem and strategy, validates the optimized results using high-fidelity CFD, and provides a systematic analysis and discussion of the rotor aerodynamic design optimization results. A comparison with the Kriging surrogate-based design optimization method is also conducted to evaluate the optimization quality and efficiency of the proposed method. Section 5 summarizes the entire work, and Section 6 points out directions for future research.

2. Improvements to the Multi-Fidelity Neural Network Model

2.1 Improvement Measures

Chen et al. [12] proposed an Adaptive Multi-Fidelity Deep Neural Network (AMF-DNNs) model building on the work of Meng et al. [11]. This model introduces a new learnable hyperparameter into the loss function, enabling adaptive identification and balancing of the linear and nonlinear relationships between high- and low-fidelity data. The specific form of the model's loss function is as follows:

$$Loss = Loss_L + Loss_{H1} + Loss_H + Loss_\lambda \tag{1}$$

where, $Loss_L$, $Loss_H$ are the loss functions of the low-fidelity and high-fidelity neural networks, respectively, $Loss_{H1}$ is a loss term used to characterize the linear relationship between low- and high-fidelity data and $Loss_\lambda$ is the regularization term, and their detailed expressions are as follows:

$$\begin{aligned}
Loss_L &= \frac{1}{N_L}\sum_{i=1}^{N_L}\left(y_L^* - y_L\right)^2 \\
Loss_{H1} &= \frac{1}{N_H}\sum_{i=1}^{N_H}\left(y_{H1} - y_H\right)^2 \\
Loss_H &= \frac{1}{N_H}\sum_{i=1}^{N_H}\left(y_H^* - y_H\right)^2 \\
Loss_\lambda &= \lambda\left(\sum_i \theta_{L,i}^2 + \sum_j \theta_{H2,j}^2\right) \\
y_H^* &= y_{H1} + \alpha y_{H2} \\
\alpha &= 1 - e^{-\beta Loss_{H1}}
\end{aligned} \tag{2}$$

where, N_L is the number of low-fidelity data, y_L^* is the predicted value of x_L obtained through the low-fidelity neural network; N_H is the number of high-fidelity data, y_{H1} is the predicted value of x_H obtained through the linear high-fidelity neural network, y_{H2} is the predicted value of x_H obtained through the nonlinear high-fidelity neural network; $\{\theta_{L,i}\}$ denotes all parameters in the low-fidelity neural network, and $\{\theta_{H2,i}\}$ denotes all parameters in the nonlinear high-fidelity neural network, λ is the regularization coefficient; α is a hyperparameter introduced related to $Loss_{H1}$, β is a parameter that controls the influence of $Loss_{H1}$. The role of introducing $Loss_{H1}$ into the loss function is as follows: when the relationship between high- and low-fidelity data is linear, $Loss_{H1}$ approaches 0 and the hyperparameter α approaches 0; in this case, the model automatically weakens the influence of the nonlinear loss term and focuses more on capturing the linear correlation. When the relationship is nonlinear, $Loss_{H1}$ approaches a positive constant and α is greater than 0, thus enhancing the

nonlinear modeling capability and enabling the model to adaptively concentrate on learning the nonlinear correlation. However, in practical case tests, if only the Adam optimizer is used for training, AMF-DNNs still struggle to achieve sufficient fitting when facing complex nonlinear relationships. To address this problem, this paper investigates improvement methods from two aspects: the network architecture and the loss function.

First, given the low cost of acquiring low-fidelity data, we independently train the low-fidelity neural network model. This model aims to achieve reasonably accurate predictions for the low-fidelity case and to prevent error accumulation in subsequent steps, thereby laying a foundation for improving the accuracy of the overall multi-fidelity neural network model. Its architecture is shown in Figure 1.Once the agreement between the predictions of the low-fidelity neural network and the actual low-fidelity data meets the preset requirement, we proceed to train the high-fidelity neural network model. This step enables synergistic optimization across different fidelity levels and enhances the overall performance.

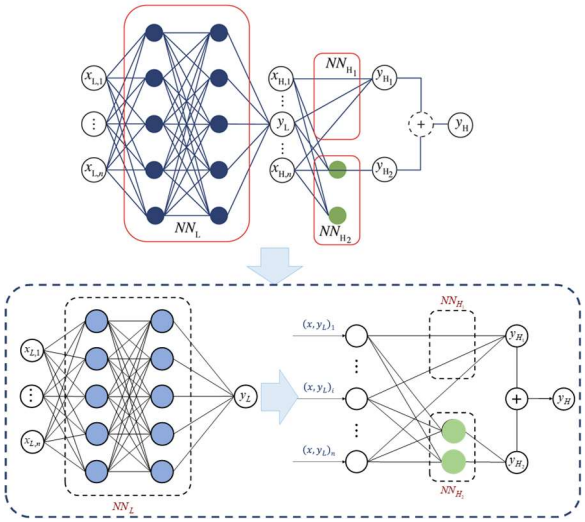


Figure 1 - Modified architecture of the multi-fidelity neural network model.

Second, in terms of the loss function, the initial loss function of the model is set as follows:

$$
\begin{aligned}
Loss &= Loss_{H_1} + Loss_H + Loss_\lambda \\
Loss_{H_1} &= \frac{1}{N_H}\sum_{i=1}^{N_H}(y_{H_1}^* - y_H)^2 \\
Loss_H &= \frac{1}{N_H}\sum_{i=1}^{N_H}(y_H^* - y_H)^2 \\
Loss_\lambda &= \lambda\sum_i \theta_{H_2,i}^2 \\
\alpha &= 1 - e^{-\beta Loss_{H_1}} \\
y_H^* &= y_{H_1} + \alpha y_{H_2}
\end{aligned}
\tag{3}
$$

After the model has preliminarily learned the approximate relationship (including both linear and nonlinear components) between the high- and low-fidelity data, the hyperparameter α obtained from this training stage is fixed and denoted as α*, and *(1-α*)* is incorporated into the loss function as a weighting parameter for the linear constraint term. The improved loss function is as follows:

$$
\begin{aligned}
Loss &= (1-\alpha^*)Loss_{H_1} + Loss_H + Loss_\lambda \\
Loss_{H_1} &= \frac{1}{N_H}\sum_{i=1}^{N_H}(y_{H_1}^* - y_H)^2 \\
Loss_H &= \frac{1}{N_H}\sum_{i=1}^{N_H}(y_H^* - y_H)^2 \\
Loss_\lambda &= \lambda\sum_i \theta_{H_2,i}^2 \\
y_H^* &= y_{H_1} + \alpha^* y_{H_2}
\end{aligned}
\tag{4}
$$

The main advantage of this improvement lies in its adaptive adjustment mechanism: when the actual relationship between the high- and low-fidelity data is linear, α^* approaches 0, and the influence of the linear constraint term is weak, so the model can still maintain a good fit to the linear relationship; when the relationship exhibits significant nonlinearity, α^* approaches 1, which effectively suppresses the influence of the linear constraint term, thereby mitigating the tendency of the model to shift toward the linear relationship in subsequent training and making it more conducive to accurately capturing and representing the complex nonlinear mapping between high- and low-fidelity data. This modified multi-fidelity neural network model is referred to as Self-Tuning Multi-Fidelity Neural Networks (ST-MFNNs).

2.2 Model Validation

In the first test case, the correlation between the high- and low-fidelity data is a one-dimensional linear function with a discontinuity. The mathematical expressions of the low- and high-fidelity functions are as follows:

$$
\begin{aligned}
y_L &= \begin{cases} 0.5(6x-2)^2\sin(12x-4)+10x-10 & 0\le x\le 0.5 \\ 0.5(6x-2)^2\sin(12x-4)+10x-7 & 0.5\le x\le 1 \end{cases} \\
y_H &= \begin{cases} (6x-2)^2\sin(12x-4) & 0\le x\le 0.5 \\ \sin(12x-4)+10 & 0.5\le x\le 1 \end{cases}
\end{aligned}
\tag{5}
$$

The training set contains a total of 6 high-fidelity sample points and 40 low-fidelity sample points. The model fitting results are shown in Figure 2, and the fitting accuracy is presented in Table 1. The results of this function test case demonstrate that, with the same number of high- and low-fidelity samples, ST-MFNNs achieve higher prediction accuracy near the discontinuity and are closer to the true high-fidelity function, compared with AMF-DNNs.

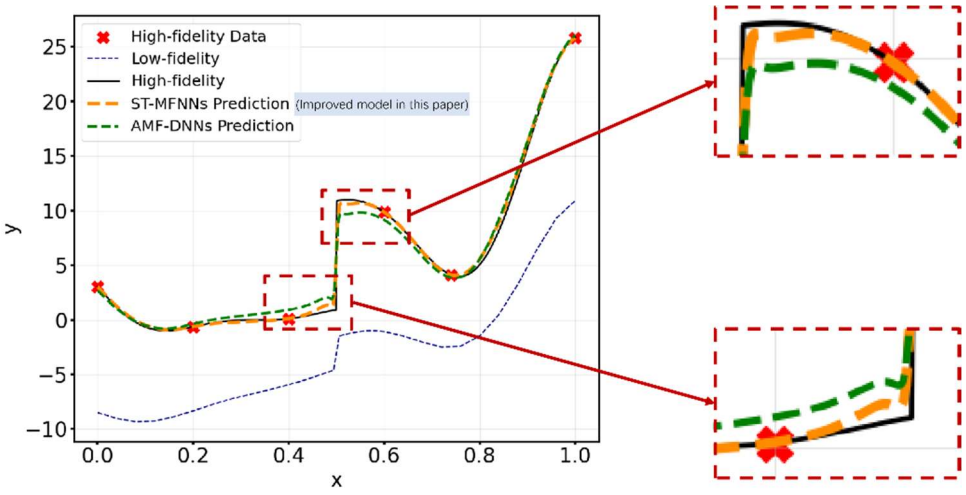


Figure 2 - Comparison of the true function and the neural network model fitting results.

Table 1 - Comparison of prediction accuracy of the neural network models.

Performance metrics	ST-MFNNs (Improved model in this paper)	AMF-DNNs
R^2	0.9950	0.9893
MSE	0.2443	0.5270
MAE	0.2891	0.5816

In the second test case, the correlation between the high- and low-fidelity data is a nonlinear function. The mathematical expressions of the low- and high-fidelity functions are as follows:

$$\begin{aligned} y_L &= \sin(8\pi x) \qquad x \in [0,1] \\ y_H &= (x-\sqrt{2})y_L^2 \end{aligned} \tag{6}$$

The training set contains a total of 15 high-fidelity samples and 51 low-fidelity samples. The model fitting results are shown in Figure 3, and the model fitting accuracy is presented in Table 2. The results of this test case demonstrate that, under the same number of high- and low-fidelity samples, compared with AMF-DNNs, the ST-MFNNs achieve higher prediction accuracy at the function peak and are closer to the true high-fidelity function.

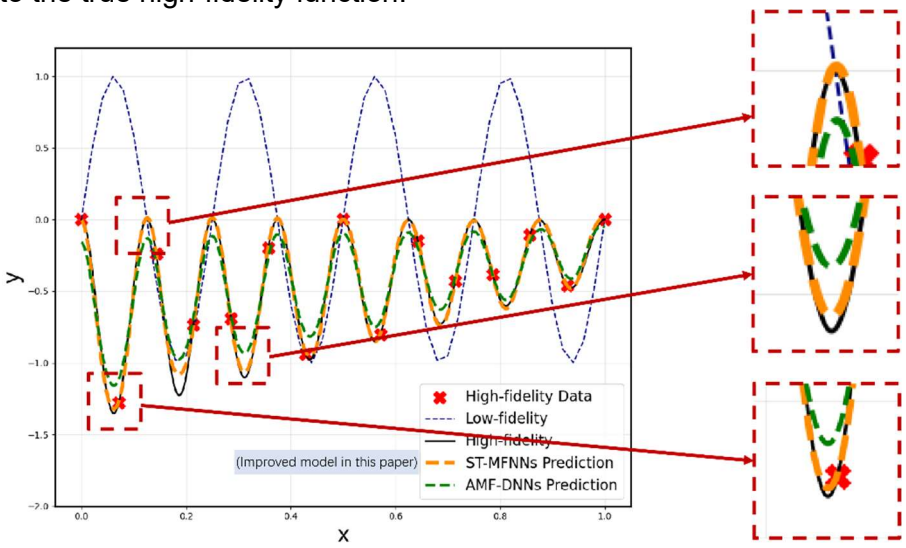


Figure 3 - Comparison of the true function and the neural network model fitting results.

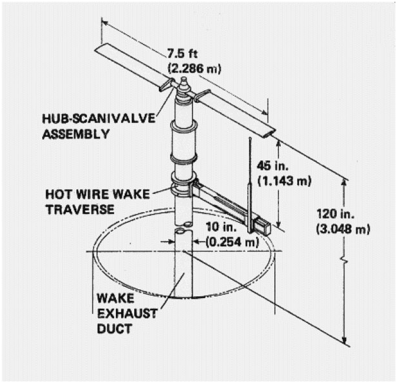
Table 2 - Comparison of prediction accuracy of the neural network models.

Performance metrics	ST-MFNNs (Improved model in this paper)	AMF-DNNs
R^2	0.9912	0.9332
MSE	0.0012	0.0091
MAE	0.0221	0.0768

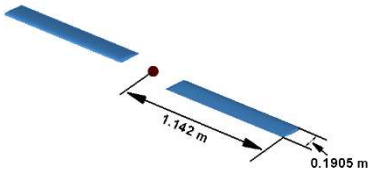
3. Modeling Method for Rotor Performance Prediction

3.1 High-Fidelity CFD Method Validation

The C-T rotor in hover is one of the standard validation cases in rotor CFD research. To verify the reliability of the numerical method adopted, this section selects this model for validation. The C-T rotor features a two-blade configuration, with blades of an untwisted, untapered rectangular planform, a cross-sectional airfoil of NACA0012, and an aspect ratio of 6. Figure 4 shows the experimental model of this rotor and the simplified model employed in the numerical calculations, respectively.



(a) Experimental model [13].



(b) Simplified computational model.

Figure 4 - Caradonna rotor model.

The computations are performed using the aerodynamic performance prediction code ROTNS for rotors in hover using overset grids developed by our research group, with the S-A turbulence model employed. The time discretization adopts the fully implicit dual-time-stepping LU-SGS method, and the spatial discretization uses the Jameson's central scheme. The computational grid is set as follows: the number of background grid cells is 100×120×100, and a C-H type grid is used for each blade with 121×49×101 cells, resulting in a total cell number of approximately 3.6 million.

In hover, if the absolute motion of the airflow is observed in a non-inertial coordinate system fixed to the rotating blade, the flow around the blade can be treated as a quasi-steady flow, thereby significantly reducing the computational requirements. Consequently, only a single blade needs to be modeled in the rotor numerical simulation, and the aerodynamic influence of the remaining blades is accounted for through rotational periodic boundary conditions. The rotational periodic boundary surfaces are shown in Figure 5. To accurately capture the blade tip vortex structure and effectively implement the rotational periodic boundary conditions, an overset grid system as shown in Figure 6 is adopted, which consists of an H-H type background grid and a C-H type blade grid. In this system, the grid points on the two rotational periodic surfaces of the background grid correspond one-to-one, facilitating the imposition of the periodic boundary conditions; the blade grid can effectively simulate viscous flows and capture the near-field wake vortex.

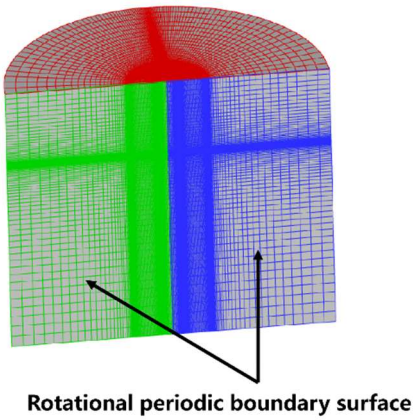


Figure 5 - Schematic of the rotational periodic boundary surfaces.

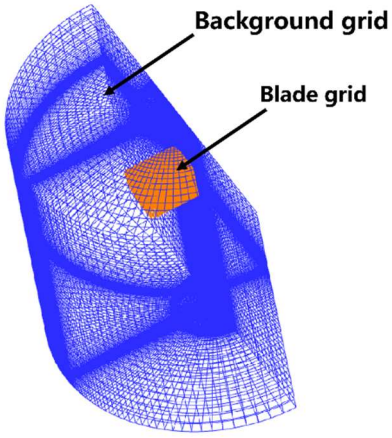
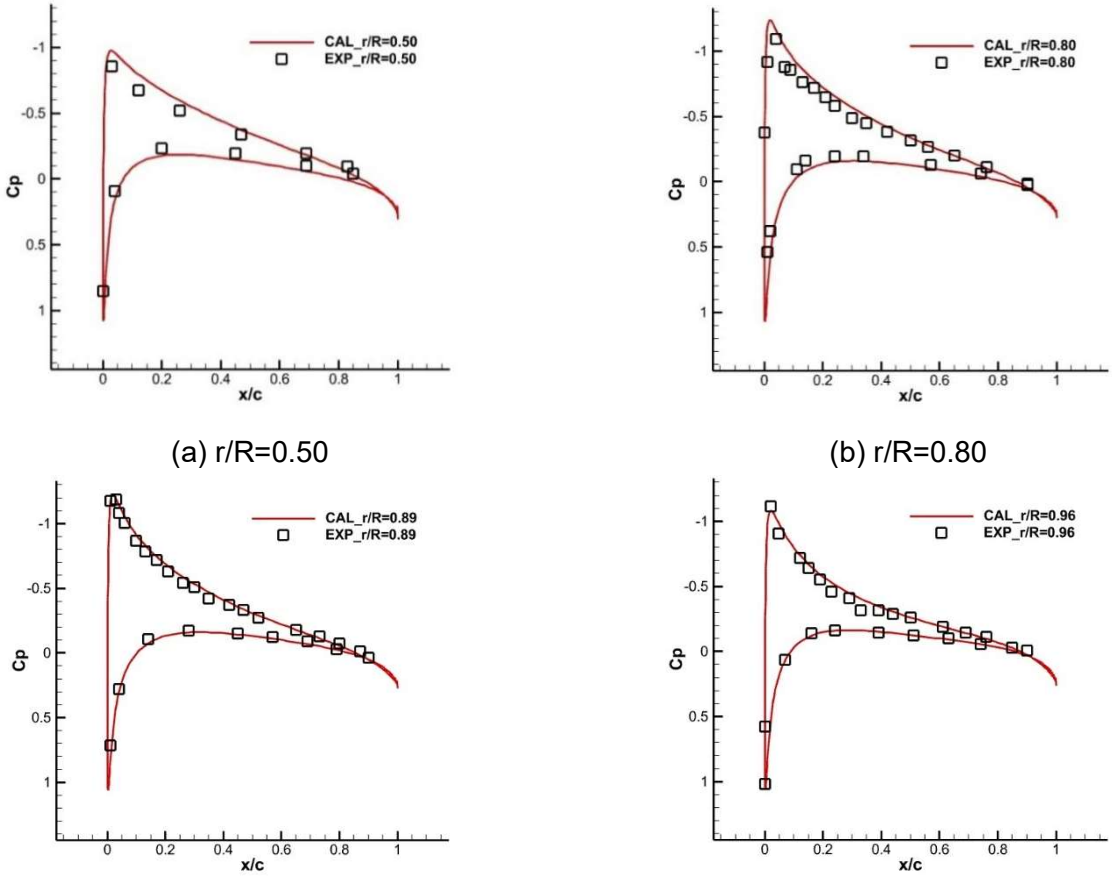


Figure 6 – Overset grid system.

The computational state parameters are as follows: Ma=0.439, Re=1.92×10^6, θ=8°. Figure 7 shows the comparison between the computed and experimental pressure distributions at different spanwise locations. The analysis results indicate that the computed curves are in good agreement with the experimental data, demonstrating that the rotor numerical simulation method adopted in this paper

can effectively capture the main physical features of the flow field pressure distribution under hover conditions and possesses good computational accuracy and reliability. This validates the effectiveness of the method and provides a reliable foundation for subsequent aerodynamic analysis, performance prediction, and aerodynamic modeling work.



(a) r/R=0.50 (b) r/R=0.80

(c) r/R=0.89 (d) r/R=0.96

Figure 7 - Comparison of computed and experimental pressure distributions at different spanwise locations for the C-T rotor in hover.

3.2 Dataset Construction

To apply the above multi-fidelity neural network modeling method to rotor aerodynamic performance prediction, it is first necessary to construct the multi-fidelity dataset required for neural network modeling. For a 5-blade rotor with a radius of 8.18m, at a tip Mach number of Ma=0.635 and a pitch angle of 11°, the helicopter rotor shape parameters were perturbed using the Latin hypercube sampling method, successfully generating 1900 different configurations. The helicopter rotor shape parameters include the blade chord distribution, twist distribution, forward/backward sweep distribution, and dihedral/anhedral distribution, totaling 17 parameters. Subsequently, the blade element momentum theory (BEMT) and the CFD method were employed to compute the performance parameters of the 1900 configurations, including thrust, torque, and moment coefficient. The grid configuration was as follows: the number of background grid cells was 100×120×100, and a C-H type grid was used for each blade with 121×49×101 cells, resulting in a total cell number of approximately 9.0 million. The rotor overset grid system is shown in Figure 8.

A total of 1900 high-fidelity and 1900 low-fidelity data points were obtained from the final calculations, from which 1500 samples were randomly selected as the training set and 400 samples as the test set.

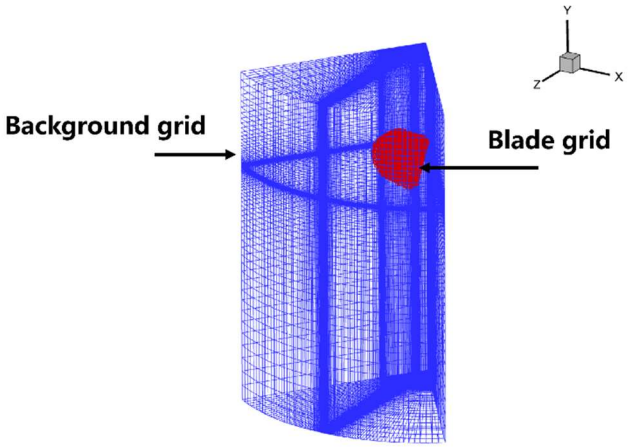


Figure 8 - Schematic of the rotor overset grid system.

In the construction and training of the multi-fidelity neural network model, the following strategy was adopted to balance computational efficiency and model accuracy: considering that the low-fidelity analysis method BEMT is computationally inexpensive, and in order to reduce the additional error accumulation that could be introduced by separately building a low-fidelity neural network, this study did not establish a low-fidelity network model; instead, the BEMT method was directly used to generate the low-fidelity data.

3.3 Model Architecture and Training Results

In the multi-fidelity neural network model, the input features are the rotor shape parameters and the low-fidelity performance parameters computed by BEMT, and the output features are the high-fidelity performance parameters. In the neural network architecture, the linear neural network part uses one hidden layer with a width of 20 and no activation function; the nonlinear neural network employs three hidden layers, each with a width of 64, and the ReLU activation function is selected. The model is trained using the Adam optimizer for 10,000 steps to obtain the hyperparameter α value at that stage, which is then incorporated into the loss function as a new parameter. Training continues with the Adam optimizer for another 10,000 steps at a learning rate of 0.001. Meanwhile, to prevent overfitting, L2 regularization is added to the nonlinear neural network part with a regularization coefficient of 0.01.

Figure 9, Figure 10 and Figure 11 show the comparison between the predicted values and the true values of rotor thrust, torque, and pitching moment coefficient in the training and test sets, respectively. It can be observed from the figures that the neural network model predictions are in close agreement with the true values, with both distributed near the main diagonal, indicating that the model possesses good overall fitting and generalization capability.

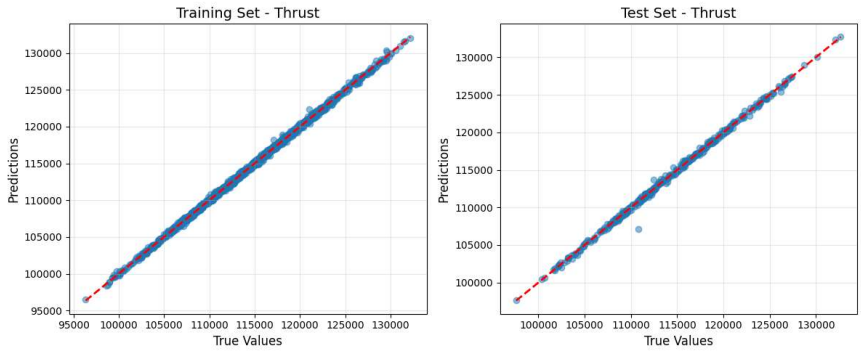


Figure 9 - Comparison of predicted and true values of thrust.

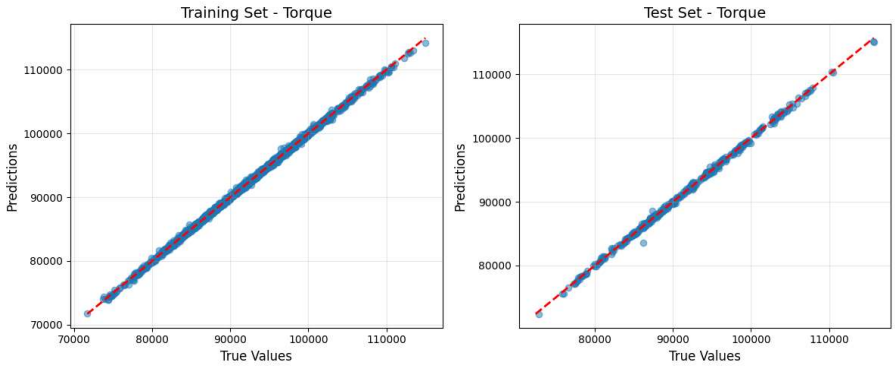


Figure 10 - Comparison of predicted and true values of torque.

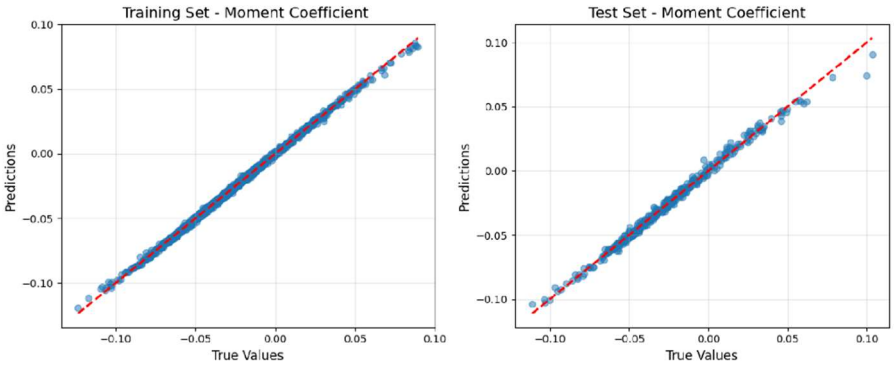


Figure 11 - Comparison of predicted and true values of moment coefficient.

Table 3 further presents the quantitative evaluation results of the prediction accuracy for the above three performance metrics on both the training and test sets. The data indicate that, whether on the training set used for model fitting or on the test set used for evaluating generalization capability, the prediction errors for all metrics remain at a low level, exhibiting a high coefficient of determination (R^2) and small root mean square error (RMSE) as well as mean absolute error (MAE). This fully validates that the constructed multi-fidelity neural network model possesses high reliability and of practical engineering value, capable of providing robust surrogate model for the subsequent rotor shape design optimization.

Table 3 - Prediction accuracy for different aerodynamic performance metrics. The RMSE and MAE are reported in the same units as the respective physical quantities, while R^2 is dimensionless.

Metric	Dataset	RMSE	MAE	R^2
Thrust (N)	Training set	200.892180	153.099838	0.998978
	Test set	297.366593	180.464478	0.997877
Torque (N·m)	Training set	220.558294	167.018570	0.999141
	Test set	277.182828	191.855804	0.998709
Moment Coefficient (-)	Training set	0.001177	0.000859	0.998645
	Test set	0.002898	0.001976	0.992459

4. Rotor Aerodynamic Shape Design Optimization Based on ST-MFNNs

4.1 Optimization Framework and Procedure

Figure 12 shows the flowchart of the rotor design optimization based on ST-MFNNs. The optimization adopts the genetic algorithm (GA), with the specific procedure as follows:

1) According to the rotor design specifications, a mathematical model comprising the objective function and constraints is established, and the ranges of the design variables are explicitly defined. Meanwhile, the genetic algorithm parameters, including population size, maximum number of generations, crossover probability and mutation probability, are set to construct the complete

optimization framework.

2) Real-number encoding is adopted to map the design variables onto chromosomes, forming a numerical representation of the solutions that serve as the basic units for subsequent genetic operations.

3) The Latin hypercube sampling method is used to generate the initial population. Each solution is termed an “individual” and is represented by a single chromosome.

4) The chromosomes are decoded into actual design variables and fed into the multi-fidelity neural network model for rotor performance calculation. Based on the objective function value and the degree of constraint violation (handled by the penalty function method), the fitness value of each individual is comprehensively computed.

5) After the fitness evaluation is completed, population iterative evolution is realized through tournament selection, blend crossover, and Gaussian mutation operations in sequence. The newly generated offspring are evaluated again, and this cycle is repeated until convergence is achieved or the preset number of iterations is reached, thus completing the optimization.

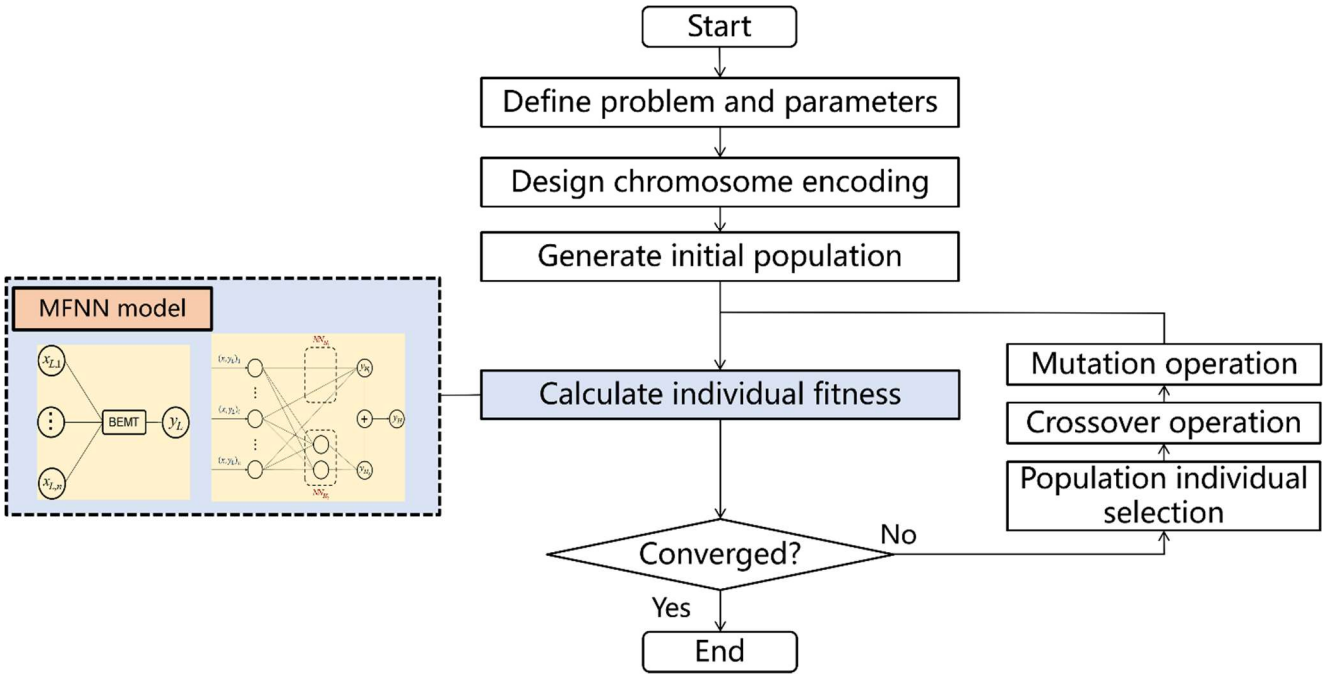


Figure 12 - Flowchart of rotor optimization based on the multi-fidelity neural network model.

4.2 Optimization Problem Formulation

The optimization problem in this paper is addressed for a 5-blade rotor with a radius of 8.18 meters. Figure 13 shows the surface pressure contour of the baseline rotor, while Figure 14 and Figure 15 present the specific twist distribution and chord distribution of the baseline rotor, respectively.

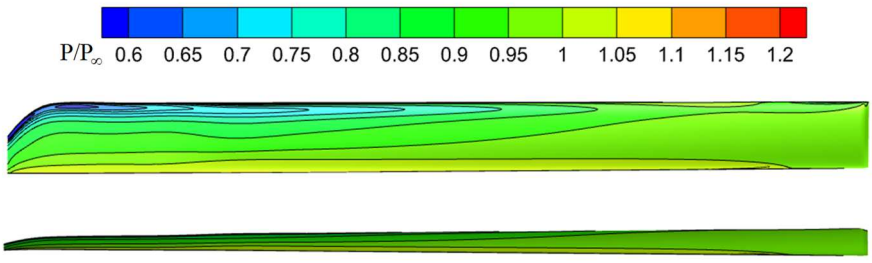


Figure 13 - Surface pressure contour of the baseline rotor.

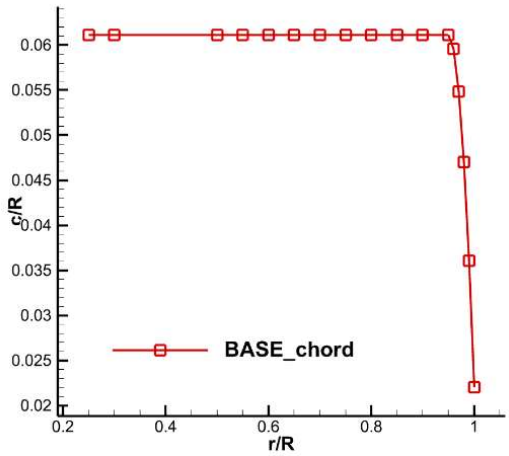


Figure 14 - Baseline rotor chord distribution.

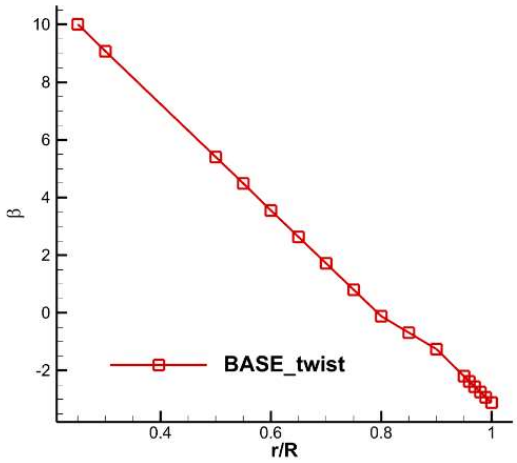


Figure 15 - Baseline rotor twist distribution.

The rotor aerodynamic design optimization takes the rotor figure of merit as the optimization objective, with the rotor thrust, moment coefficient, and solidity as constraints. The mathematical optimization model is as follows:

$$\begin{aligned} \min. \quad & -\eta_s \\ s.t. \quad & T_s - 0.95T_0 \geq 0 \\ & \left|Cm\right| \leq \left|Cm_0\right| \\ & 0.98 \leq \frac{\sigma_s}{\sigma_0} \leq 1.02 \end{aligned} \tag{7}$$

where, η_s denotes the figure of merit of the rotor in hover; T_s, σ_s and Cm denote the rotor thrust, solidity, and pitching moment coefficient about the feathering axis, respectively; and T_0, σ_0 and Cm_0 denote those of baseline rotor, respectively. The rotor aerodynamic optimization problem employs 17 design variables, including the blade chord distribution, twist angle distribution, blade tip forward/backward sweep distribution, and blade tip dihedral/anhedral distribution. The definition and the range of each design variable are presented in Table 4.

4.3 Optimization Strategy and Settings

The genetic algorithm (GA) is adopted as the optimization algorithm. The population size is set to 200 and generated via Latin hypercube sampling. The optimization runs for 100 generations. Simulated binary crossover (SBX) is used with a crossover probability of 0.7 and a distribution index of 15, while polynomial mutation is applied with a mutation probability of 0.3 and a distribution index of 20. The penalty function method is used for constraint handling.

4.4 Optimization Results (Validated by High-Fidelity CFD)

Table 5 compares the aerodynamic performance of the baseline and optimized rotors, where “BASE” denotes the baseline rotor and “OPT-ST-MFNNs” denotes the optimized one. All results of aerodynamic performance are computed using the high-fidelity CFD method. It can be observed that, under the given constraints, the rotor figure of merit improves from 69.53% (baseline) to 72.57%.

Table 4 - Design variable definitions and ranges.

Variable	Description	Range
DV1	Chord length at blade root (0.25R)	0.40≤DV1≤0.50
DV2	Chord length at blade mid-span (0.50R)	0.40≤DV2≤0.55
DV3	Location of maximum chord	0.70≤DV3≤0.80
DV4	Maximum chord length	0.50≤DV4≤0.63
DV5	Chord length at blade tip (1.00R)	0.135≤DV5≤0.18
DV6	Twist angle at blade root	9.50≤DV6≤10.50
DV7	Twist rate from 0.2R to 0.8R	2.10≤DV7≤2.40
DV8	Twist rate from 0.8R to 0.9R	1.30≤DV8≤1.50
DV9	Twist rate from 0.9R to R	2.10≤DV9≤2.40
DV10	Forward sweep onset location	0.75≤DV10≤0.85
DV11	Backward sweep onset location	0.85 ≤DV11≤0.95
DV12	Forward sweep angle	0≤DV12≤10
DV13	Backward sweep angle	0≤DV13≤30
DV14	Dihedral onset location	0.75 ≤DV14≤0.85
DV15	Anhedral onset location	0.85 ≤DV15≤0.95
DV16	Dihedral angle	0≤DV16≤10
DV17	Anhedral angle	0≤DV17≤10

Figure 16 and Figure 17 compare the blade shape and contour of the baseline and optimized rotor. It can be observed that the optimized rotor blade has reduced chord lengths at the root and tip and increased chord length in the middle section; the outboard section features large backward sweep and anhedral, while the inboard section is supplemented with slight forward sweep and dihedral. From the perspective of mechanism analysis, the optimized rotor achieves tip off-loading through the large backward sweep in the outboard section, weakening the blade tip vortex strength to reduce induced losses; meanwhile, the outboard anhedral increases the vertical distance between the tip vortex and the rotor disk, thereby mitigating the close-range induced interference of the tip vortex on the rotor disk. However, while the large backward sweep and anhedral in the outboard section reduce induced losses, they also lead to a decrease in the lift contribution of the outboard section. Therefore, to compensate for the outboard lift loss, the chord length in the mid-span section is increased to enhance thrust, and slight forward sweep and dihedral are applied in the inboard section to balance the load distribution, thereby achieving an overall improvement in the figure of merit.

Table 5 - Comparison of rotor performance before and after optimization.

	C_t	C_p	$\lvert C_m \rvert$	FM
BASE	0.018909	0.0018645	0.01092	69.53%
OPT-ST-MFNNs	0.019255	0.0018408	0.00820	72.57%

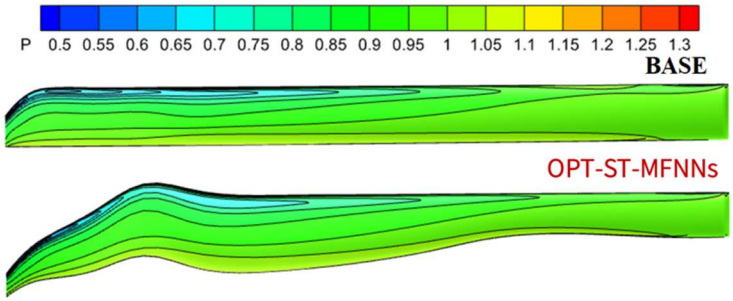


Figure 16 - Comparison of rotor surface pressure contours before and after optimization (XOZ plane).

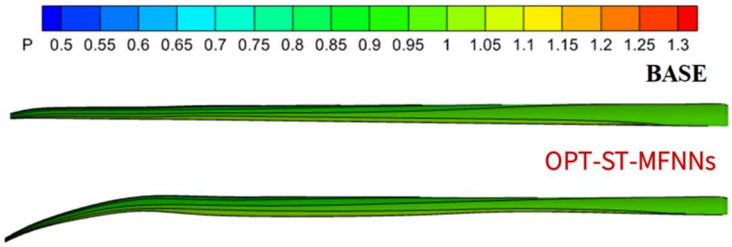


Figure 17 - Comparison of rotor surface pressure contours before and after optimization (YOZ plane).

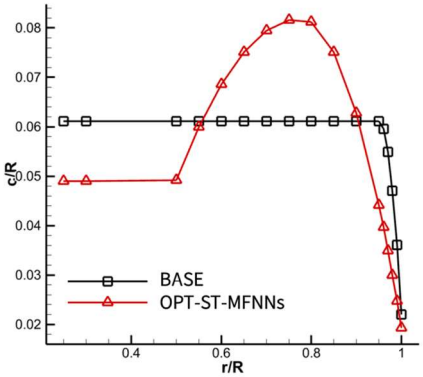


Figure 18 - Comparison of rotor chord distribution before and after optimization.

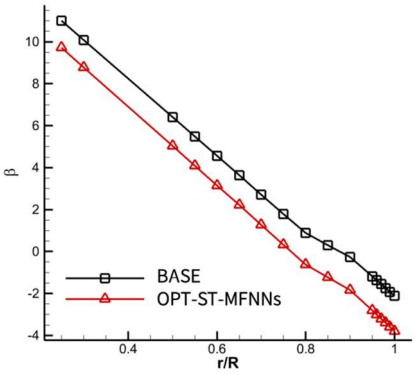


Figure 19 - Comparison of rotor twist distribution before and after optimization.

To verify the reliability of the developed method, the surrogate-based global optimization method using the Kriging model is selected as the comparative method [8]. Figure 20 and Figure 21 compare the rotor surface pressure contours obtained by the two optimization methods, and Figure 22 compares the chord and twist distributions of the optimized rotors obtained by the two methods, where “OPT-Kriging” denotes the optimization result based on the Kriging model, and “OPT-ST-MFNNs” denotes the optimization result based on ST-MFNNs. It can be observed that OPT-ST-MFNNs exhibits strong agreement with OPT-Kriging, especially in critical geometric characteristics, including chord distribution along the span, twist angle variation, and blade tip sweep (forward/backward) and dihedral/anhedral.

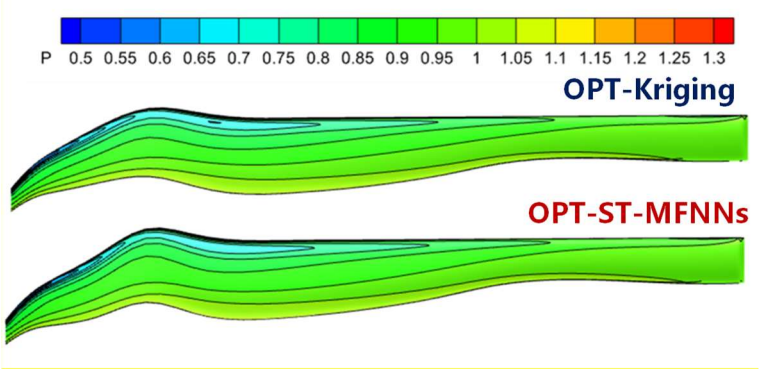


Figure 20 - Comparison of rotor surface pressure contours obtained by the two optimization methods (XOZ plane).

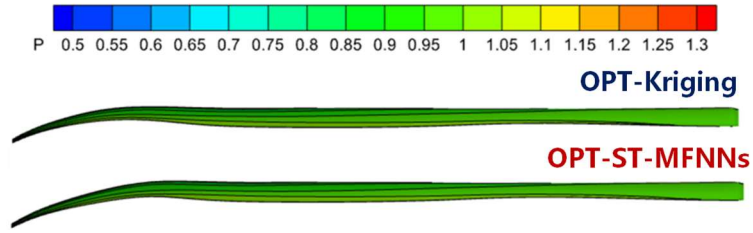


Figure 21 - Comparison of rotor surface pressure contours obtained by the two optimization methods (YOZ plane).

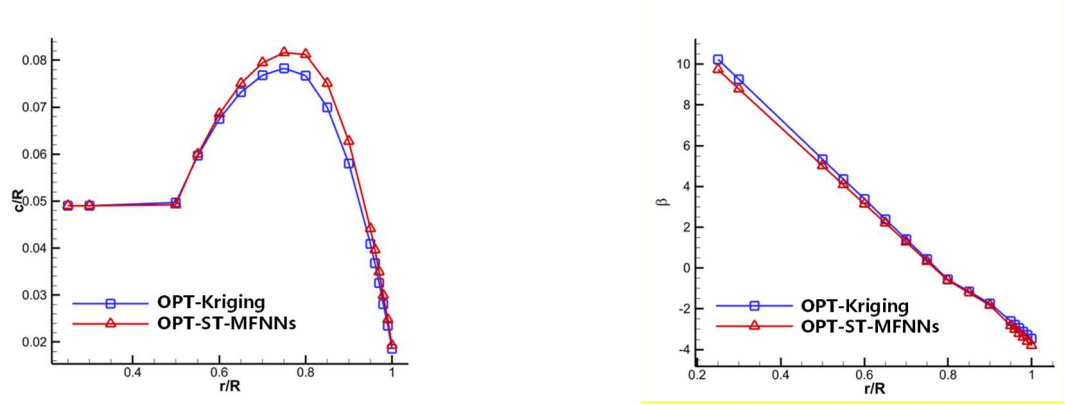


Figure 22 - Comparison of rotor chord/twist distributions by the two optimization methods.

Table 6 further compares the aerodynamic performance of the optimized rotors obtained by the two optimization methods. The results of aerodynamic performance are all computed using the high-fidelity CFD method. The data show that the aerodynamic performances of the two optimized results are very close, with a difference in figure of merit of only -0.08%, indicating that the rotor aerodynamic design optimization method based on ST-MFNNs proposed in this paper has high credibility and practical value.

Table 6 - Comparison of optimized rotor performance obtained by the two optimization methods.

	C_t	C_p	$\lvert C_m \rvert$	FM
OPT-Kriging	0.019023	0.0018054	0.00815	72.65%
OPT-ST-MFNNs	0.019255	0.0018408	0.00820	72.57%

Table 7 compares the time consumption of the two optimization methods. The surrogate-based optimization method using the Kriging model took a total of 363.54 hours for the optimization process, whereas the ST-MFNNs method reduced the optimization time to 4.4 hours, achieving an improvement in computational efficiency by a factor of approximately 82.5. Even when the time required for

constructing the neural network dataset is included, the overall optimization cycle is only 22.4 hours, still representing an efficiency improvement by a factor of about 16. This indicates that the optimization design method based on the multi-fidelity neural network proposed in this paper can significantly accelerate the rotor design optimization process, substantially reducing the time cost while ensuring computational accuracy. All computations in this study were performed on a computer equipped with an Intel Core i9-13900K CPU.

Table 7 - Comparison of optimization time between the two optimization methods.

Solver	Optimization time (hours)	Speedup
Kriging-CFD	363.54	1×
ST-MFNNs	4.4	82.5×
ST-MFNNs (including dataset construction)	22.4	16×

5. Conclusions

Addressing the core contradiction between accuracy and efficiency in helicopter rotor design optimization, this paper proposes a multi-fidelity neural network modeling method with higher accuracy and stronger robustness, and successfully applies it to rotor aerodynamic design optimization. The main research achievements and conclusions are as follows:

(1) A multi-fidelity neural network modeling method with higher accuracy and stronger robustness is proposed. To address the problem of insufficient accuracy of existing models in capturing the complex correlations between high- and low-fidelity data, this paper investigates improvement methods from two aspects: the network architecture and the loss function. In terms of the network architecture, an independent pre-training strategy for the low-fidelity neural network is adopted, which effectively prevents error propagation and accumulation between the high- and low-fidelity networks. In terms of the loss function, an error-related hyperparameter is introduced, enabling more precise characterization and balancing of linear and nonlinear correlations. Validation through two typical numerical test cases demonstrates that the improved model (ST-MFNNs) significantly outperforms existing methods (e.g., AMF-DNNs) in both prediction accuracy and robustness, with particular advantages in scenarios involving function discontinuities and high peaks.

(2) A multi-fidelity neural network prediction model for helicopter rotor aerodynamic performance is constructed. Taking a five-bladed rotor with a blade radius of 8.18m as the research object, a multi-fidelity dataset is established based on the blade element momentum theory (BEMT) and the high-fidelity CFD method, respectively. Using this dataset, a multi-fidelity neural network model for rotor aerodynamic performance is trained based on ST-MFNNs. It is verified that the prediction results are very close to the high-fidelity CFD results, meeting the accuracy requirements, thus laying a solid foundation for subsequent efficient and reliable rotor aerodynamic design optimization.

(3) A high-efficiency and high-precision rotor aerodynamic optimization design method based on a multi-fidelity neural network is proposed. A Kriging-based optimization method with high efficiency and global search capability is selected for comparison. Targeting a rotor with a radius of 8.18m and aiming to maximize the figure of merit, 17 aerodynamic shape parameters of the rotor are optimized. The results show that the optimized rotor shapes and aerodynamic performances obtained by the two methods are highly consistent. Compared with the Kriging-based optimization, the computational efficiency is improved by a factor of 82.5. Even when accounting for the dataset construction time, the efficiency is improved by a factor of 16.

6. Outlook

Nevertheless, the current research still has limitations. In future studies, we plan to pursue further developments in the following aspects:

(1) Extending the proposed method to rotor optimization involving complex flight conditions and dynamic maneuvers, such as forward flight and descending flight. Under these conditions, conventional CFD methods consume substantial time and computational resources, whereas the neural network approach can keep resource consumption within an engineering-acceptable range.

(2) Extending the proposed method to multidisciplinary coupled optimization of rotor aerodynamics,

structures, and noise. In actual operation, the rotor is subject to multi-physics coupling. In the future, structural dynamics models (e.g., vibration and dynamic loads) can be introduced to establish a multi-fidelity aerodynamics–structures–acoustics collaborative optimization framework, thereby improving the overall performance and reliability of the rotor.

(3) Integrating physics-informed neural networks (PINNs) with multi-fidelity models. PINNs enhance extrapolation and prediction capabilities in data-scarce regions by embedding governing equations. By combining low-fidelity models or simplified physical equations, a physics–data dual-driven hybrid model can be constructed to further improve generalization ability and design space exploration efficiency.

7. Acknowledgment

This work was supported by the National Key Research and Development Program of China under Grant No. 2023YFB3002800.

We gratefully acknowledge the Computing Center in Xi'an for providing computational resources.

8. Contact Author Email Address

Wenping Song: wpsong@nwpu.edu.cn

9. Copyright Statement

The authors confirm that they, and/or their company or organization, hold copyright on all of the original material included in this paper. The authors also confirm that they have obtained permission, from the copyright holder of any third party material included in this paper, to publish it as part of their paper. The authors confirm that they give permission, or have obtained permission from the copyright holder of this paper, for the publication and distribution of this paper as part of the ICAS proceedings or as individual off-prints from the proceedings.

References

[1] Wu X M and Mu X W. A perspective of the future development of key helicopter technologies. *Acta Aerodynamica Sinica*, Vol. 39, No. 3, pp 1-10, 2021. (in Chinese)

[2] Xiong H J. Overview of helicopter rotor system configuration development. *Flight Dynamics*, Vol. 223, No. 1, pp 61-66, 2025. (in Chinese)

[3] Adelman H M and Mantay W R. Integrated multidisciplinary design optimization of rotorcraft. *Journal of Aircraft*, Vol. 28, No. 1, pp 22-28., 1991.

[4] Khan A M. Helicopter mission and rotor performance optimization with quasi-linear inflow theory. PhD thesis, Georgia Institute of Technology, Atlanta, 1992.

[5] Quackenbush T R, Wachspress D A and Kaufman A. E. Optimization of rotor performance in hover using a free wake analysis. *Journal of Aircraft*, Vol.28, No. 1, pp 200-206, 1991.

[6] Yang C, Aoyama T and Chae S. Blade planform optimization to reduce HSI noise of helicopter in hover. *Annual Forum Proceedings-AHS International*, American Helicopter Society, Vol. 3, pp 2218-2232, 2008.

[7] Qian R Z, Qiao Z D, Chen Y C and Zhao K L. Rotor Airfoil Optimization Design Using Navier-Stokes Equations. *Flight Dynamics*, Vol. 22, No. 1, pp 26-29, 2004. (in Chinese)

[8] Bu Y P, Song W P, Han Z H, Zhang Y and Zhang L. Aerodynamic/aeroacoustic variable-fidelity optimization of helicopter rotor based on hierarchical Kriging model. *Chinese Journal of Aeronautics*, Vol. 33, No. 2, pp 476-492, 2020.

[9] Bu Y P, Song W P, Han Z H and Zhang Y. Efficient aerostructural optimization of helicopter rotors toward aeroacoustic noise reduction using multilevel hierarchical kriging model. *Aerospace Science and Technology*, Vol. 127, 107683, 2022.

[10] Zhang T, Barakos G N and Foster M. Multi-fidelity aerodynamic design and analysis of propellers for a heavy-lift eVTOL. *Aerospace Science and Technology*, Vol. 135, 108185, 2023.

[11]Meng X H and Karniadakis G E. A composite neural network that learns from multi-fidelity data: Application to function approximation and inverse PDE problems. *Journal of Computational Physics*, Vol. 401, 109020, 2020.

[12]Chen B N, Xie F F and Meng X H. Adaptive multi-fidelity composite deep neural networks. *Physics of Gases*, Vol. 9, No. 4, pp 1-8, 2024. (in Chinese)

[13]Caradonna F X and Tung C. Experimental and analytical studies of a model helicopter rotor in hover. *Vertica*, Vol. 5, No. 2, pp 149-161, 1981.